

Resonant Graviton-Photon Conversion with Stochastic Magnetic Field in the Expanding Universe

Andrea Addazi

*Center for Theoretical Physics, College of Physics,
Sichuan University, Chengdu, 610064, PR China and
INFN, Laboratori Nazionali di Frascati,
Via E. Fermi 54, I-00044 Roma, Italy*

Salvatore Capozziello

*Dipartimento di Fisica "E. Pancini", Universita di Napoli "Federico II",
and Istituto Nazionale di Fisica Nucleare,
Sezione di Napoli, Compl. Univ. di Monte S. Angelo,
Edificio G, Via Cinthia, I-80126, Napoli, Italy and
Scuola Superiore Meridionale, Largo S. Marcellino 10, I-80138, Napoli, Italy*

Qingyu Gan

Scuola Superiore Meridionale, Largo S. Marcellino 10, I-80138, Napoli, Italy

Abstract

We investigate graviton-photon oscillations sourced by cosmological magnetic fields from Gertsenshtein effect. We adopt a robust perturbative approach and we find that the conversion probability from graviton to photon can be resonantly enhanced in monochromatic, multi-chromatic and scale invariant spectrum models of stochastic magnetic field fluctuations. In addition, the expansion of the Universe acts as a decoherence factor, which demands a natural discretization scheme along the line of sight. Including also decoherence from cosmic acceleration, we find that conversion probabilities for stochastic magnetic fields are completely different than results predicted from existing magnetic domain-like models in a wide range of magnetic strengths and coherence lengths. Resonances can be tested by radio telescopes as a probe of high frequency gravitational wave sources and primordial magnetogenesis mechanisms.

Contents

I. Introduction	2
II. The Gertsenshtein Effect	4
III. Resonance	9
IV. discretization scheme	12
V. Numerical results	17
VI. Discussion and Conclusions	23
References	25

I. INTRODUCTION

In last decade, a large amount of astrophysical and cosmological data in electromagnetic (EM) and gravitational wave (GW) channels opens the possibility to test several new physics mechanisms in the early Universe from the multi-messenger approach. Intriguingly, EM and GW radiations can be entwined through the (inverse) Gertsenshtein effect. This describes a conversion between graviton and photon in the presence of a magnetic background field [1]. Such an effect can have several cosmological implications such as detecting the GW signals via radio-wave channel and vice versa [2–8], probing the primordial magnetic field [9], testing QED corrections [10–12], constraining the dark photons [13], testing the modified gravity theory [14, 15] and so on. In particular, in Ref. [7] the authors obtained the existing strongest upper bounds on the MHz-GHz primordial GWs derived from radio telescopes ARCADE 2 [16] and EDGES [17].

The magnetic background field plays a pivotal role in the Gertsenshtein mechanism. Concerning the cosmic magnetic field in intergalactic scale, its origin remains a mystery yet. The observational bounds on the strength and coherence length of intergalactic magnetic fields are obtained from Faraday rotation measures [18], CMB analysis [19], magnetohydrodynamics processes [20, 21] and blazar gamma-rays [22]. Theoretical considerations point to two typical magnetogenesis scenarios in the primordial Universe: cosmological first order phase

transitions and inflation. For phase transitions, causality bounds lead to a blue spectrum of the magnetic field. On the other hand, inflation models can generate a scale invariant spectrum. (See Ref. [23, 24] for a comprehensive review on these subjects).

The graviton-photon mixing is described by a system of equations which can be analytically solved for a constant magnetic field [25]. For the more complicated case of an inhomogeneous magnetic background, two main approaches have been proposed. The first, known as the “domain-like” model [2, 4, 26–35], assumes that the line-of-sight path can be divided into many patches with size of about the coherence length of the magnetic field. In each domain, the magnetic field is assumed to be uniform but its direction is randomly chosen. This approach is widely adopted for simplicity. On the contrary, the stochastic approach assumes that magnetic random perturbations are isotropic and Gaussian distributed. In the statistical approach, one can perform perturbative methods, starting with the power spectrum of the stochastic magnetic field and solving wave equations for perturbations around it [7, 30, 31, 36–39]. Within this framework, in Refs. [7, 38] the authors found an interesting phenomenon: graviton-photon conversion probability has a linear growth with the propagation distance. In fact, this is a parametric resonance arising from a magnetic oscillation in certain frequency which was firstly addressed in a photon-axion mixing system [36]. Moreover, similar linear amplification of the conversion probability has also been found from inhomogeneity of electron density perturbations [40]. Despite its significance, graviton-photon resonances have not received a wide attention in literature.

As mentioned above, in most of domain-like models the mean patch size is assumed to be of the order of the coherence length of the magnetic field. This can be theoretically conceivable in the causal magnetogenesis from phase transition. However, for magnetogenesis from inflation, in the case of a scale-invariant spectrum, the coherence length loses its clear physical interpretation rendering the above discretization scheme inadequate. Moreover, non-commutativity of the wave equation at different cosmic time in an expanding Universe leads to a type of decoherence effect which is commonly neglected in domain-like approaches. In general the decoherence factors for graviton-photon oscillations (e.g., the inhomogeneity of the electron density, inelastic scattering of the participating particles and so on) demands a proper discretization scheme along the line of sight.

In this paper, we will explore parametric resonances in graviton-photon transitions with cosmological stochastic magnetic fields. As mentioned above such a phenomenon was poorly

analysed in literature. We will approach the problem with perturbative methods including decoherence from cosmic acceleration with discretization scheme beyond domain-like one. In our analysis, we consider both mono-chromatic and scale-invariant power spectra of random magnetic field fluctuations. Remarkably, we will show that, in several regions of parameters, resonances can enhance graviton-photon oscillation probability up to $2 \sim 5$ orders of magnitude with respect to results given in Ref. [7]. Furthermore, resonance effects, with their distinct features, in relation to the magnetic spectrum, can be employed as valuable probes to discern the magnetogenesis models in early Universe.

Our paper is organized as follows. In Sec. II, we briefly introduce the graviton-photon mixing system in the static Universe and obtain the expression for the conversion probability in inhomogeneous magnetic background using the perturbative approach. In Sec. III, we show the parametric resonances of two representative power spectra of magnetic field. In order to account for the expansion of the Universe, we apply the discretization scheme based on steady approximation and show the numerical results in Sec. IV. In Sec. VI we show our conclusions, discussions and remarks on our results and future prospectives.

II. THE GERTSENSHTEIN EFFECT

The (inverse) Gertsenshtein effect describes the conversion between the graviton and photon in the presence of a magnetic field. As a first approximation, we assume Universe expansion as negligible and consider graviton-photon transitions in Minkowski spacetime. Let us consider gravitons propagate along the l -direction and convert to photons (we avoid using “ z -direction” as z denotes the redshift of Universe). As shown in Ref. [41], the mixing system including two polarization states of photon as well as graviton in an external magnetic background $\mathbf{B} = (\mathbf{B}_x(l), \mathbf{B}_y(l), \mathbf{B}_z(l))$ is described by

$$(\omega + i\partial_l) \mathbf{I}_{4 \times 4} \begin{pmatrix} h_{\times}(\omega, l) \\ h_{+}(\omega, l) \\ A_x(\omega, l) \\ A_y(\omega, l) \end{pmatrix} + \begin{pmatrix} 0 & 0 & -iM_{g\gamma}^x & iM_{g\gamma}^y \\ 0 & 0 & iM_{g\gamma}^y & iM_{g\gamma}^x \\ iM_{g\gamma}^x & -iM_{g\gamma}^y & M_x & M_{\text{CF}} \\ -iM_{g\gamma}^y & -iM_{g\gamma}^x & M_{\text{CF}}^* & M_y \end{pmatrix} \begin{pmatrix} h_{\times}(\omega, l) \\ h_{+}(\omega, l) \\ A_x(\omega, l) \\ A_y(\omega, l) \end{pmatrix} = 0 \quad (\text{II.1})$$

with the mixing matrix elements

$$M_{g\gamma}^x = \frac{1}{2} \kappa \mathbf{B}_x, \quad M_{g\gamma}^y = \frac{1}{2} \kappa \mathbf{B}_y, \quad M_x = -\frac{1}{2} \frac{\Pi_{xx}}{\omega}, \quad M_y = -\frac{1}{2} \frac{\Pi_{yy}}{\omega}, \quad M_{\text{CF}} = -\frac{1}{2} \frac{\Pi_{xy}}{\omega}. \quad (\text{II.2})$$

We work in Planck unit and set $\kappa = \sqrt{16\pi}$. Here, $A_{x/y}(\omega, l)$ and $h_{+/\times}(\omega, l)$ are polarized modes of photons and gravitons in frequency ω , respectively. We point out that above formula is only valid when the external magnetic field varies in space on much larger scales than the wavelength of mixing gravitons as well as photons. Although the cosmic magnetic field has not been observed yet, theoretical constraints suggest that it coherently oscillates at a certain scale larger than 1pc [23]. It indicates that Eq. (II.1) can be a good approximation since the frequency of the mixing system of our interests is typically $\omega \gtrsim$ MHz (corresponding to the wavelength \lesssim km).

Concerning the $\Pi_{xx/xy/yy}$ terms, they present the effects of the uniform plasma as well as transverse magnetic background on the polarized photons. As shown in [41, 42], the Cotton-Mouton effect due to the external magnetic field can be schematically captured in $\sim \frac{\omega_{\text{pl}}^2 \omega_c^2}{\omega^2 - \omega_c^2}$ with plasma frequency $\omega_{\text{pl}} = \sqrt{e^2 n_e / m_e}$ and cyclotron frequency $\omega_c = eB / m_e$. Here m_e , e and n_e are respectively the mass, charge and number density of the free electrons in the plasma and $B = |\mathbf{B}|$ is the strength of the magnetic field. In our setup with $\omega \gtrsim$ MHz and $B \lesssim 10^{-9}$ Gauss, the typical scales of plasma and cyclotron frequencies are $\omega_{\text{pl}} \simeq 1$ Hz and $\omega_c \lesssim 0.01$ Hz, which indicates that the Cotton-Mouton effect has little contribution to $\Pi_{xx/xy/yy}$ terms. In addition, the Faraday Rotation included in Π_{xy} term describes the coupling between two photon polarization states. It plays the role in the analysis of the conversion between two polarized modes of photons, which is irrelevant for the problem at hand. In short, we can safely neglect the Cotton-Mouton effect as well as the Faraday Rotation and only include the plasma effect as $\Pi_{xx} \simeq \Pi_{yy} \simeq \omega_{\text{pl}}^2$ and $\Pi_{xy} \simeq 0$. Then from Eq. (II.2), Eq. (II.1) can be simplified as

$$\partial_l \begin{pmatrix} h_{\times}(\omega, l) \\ h_{+}(\omega, l) \\ A_x(\omega, l) \\ A_y(\omega, l) \end{pmatrix} = iK(l) \begin{pmatrix} h_{\times}(\omega, l) \\ h_{+}(\omega, l) \\ A_x(\omega, l) \\ A_y(\omega, l) \end{pmatrix}, \quad (\text{II.3})$$

$$K(l) = \begin{pmatrix} \omega & 0 & -i\frac{1}{2}\kappa\mathbf{B}_x(l) & i\frac{1}{2}\kappa\mathbf{B}_y(l) \\ 0 & \omega & i\frac{1}{2}\kappa\mathbf{B}_y(l) & i\frac{1}{2}\kappa\mathbf{B}_x(l) \\ i\frac{1}{2}\kappa\mathbf{B}_x(l) & -i\frac{1}{2}\kappa\mathbf{B}_y(l) & \omega(1+n_{\text{pl}}) & 0 \\ -i\frac{1}{2}\kappa\mathbf{B}_y(l) & -i\frac{1}{2}\kappa\mathbf{B}_x(l) & 0 & \omega(1+n_{\text{pl}}) \end{pmatrix},$$

where we introduce the refraction index $n_{\text{pl}} = -\omega_{\text{pl}}^2 / (2\omega^2)$. To obtain the conversion proba-

bility in the graviton-photon mixing, we introduce a conversion matrix \mathcal{U} in 4×4 size given by $(h_\times(l), h_+(l), A_x(l), A_y(l))^T = \mathcal{U}(l, l_0)(h_\times(l_0), h_+(l_0), A_x(l_0), A_y(l_0))^T$. The conversion matrix $\mathcal{U}(l, l_0)$ has a clear physical interpretation as each component represents the corresponding conversion process among different polarized modes of gravitons and photons. Let us concentrate on the transition process from the gravitons to photons and assume that the GW source to be unpolarized with source's intensity normalized to unity. Thus the initial conditions are chosen to be $A_x(l_0) = A_y(l_0) = 0$, $h_\times(l_0) = c_1$ and $h_+(l_0) = c_2$, where the random complex constants statistically average to zero but their mean squares remain non-vanishing, i.e., $\langle c_1 \rangle = \langle c_2 \rangle = 0$ and $\langle |c_1|^2 \rangle = \langle |c_2|^2 \rangle = 1/2$. At distance l , the generating photons can be easily read from the conversion matrix, namely $A_x(l) = \mathcal{U}_{31}c_1 + \mathcal{U}_{32}c_2$ and $A_y(l) = \mathcal{U}_{41}c_1 + \mathcal{U}_{42}c_2$. Performing an average over the initial unpolarized GW state, we obtain the conversion probability

$$\langle \mathcal{P}(l) \rangle = \frac{\langle |A_x(l)|^2 \rangle + \langle |A_y(l)|^2 \rangle}{\langle |h_\times(l_0)|^2 \rangle + \langle |h_+(l_0)|^2 \rangle} = \frac{1}{2} (|\mathcal{U}_{31}|^2 + |\mathcal{U}_{32}|^2 + |\mathcal{U}_{41}|^2 + |\mathcal{U}_{42}|^2), \quad (\text{II.4})$$

where the interference terms (e.g., $c_1 c_2^* \mathcal{U}_{31} \mathcal{U}_{32}^*$ etc.) vanish due to $\langle c_1 \rangle = \langle c_2 \rangle = 0$.

To compute conversion matrix \mathcal{U} , we rewrite Eq. (II.3) in form of

$$\partial_l \mathcal{U}(l, l_0) = iK(l)\mathcal{U}(l, l_0). \quad (\text{II.5})$$

We firstly consider the mixing matrix K to be l -independence, which allows us to express the exact solution in a closed form $\mathcal{U}(l, l_0) = \exp[i(l - l_0)K]$. One can directly calculate $|\mathcal{U}_{31}|^2 = |\mathcal{U}_{42}|^2 = \frac{1}{4}\kappa^2 \mathbf{B}_x^2 l_{\text{osc}}^2 \sin^2((l - l_0)/l_{\text{osc}})$ and $|\mathcal{U}_{32}|^2 = |\mathcal{U}_{41}|^2 = \frac{1}{4}\kappa^2 \mathbf{B}_y^2 l_{\text{osc}}^2 \sin^2((l - l_0)/l_{\text{osc}})$, then obtain the probability of the graviton transition to photon for a traveling distance $\Delta l = l - l_0$ as

$$\langle \mathcal{P}(\Delta l) \rangle = \frac{1}{4}\kappa^2 (\mathbf{B}_x^2 + \mathbf{B}_y^2) l_{\text{osc}}^2 \sin^2(\Delta l/l_{\text{osc}}). \quad (\text{II.6})$$

Here $l_{\text{osc}} = 2/\sqrt{\kappa^2(\mathbf{B}_x^2 + \mathbf{B}_y^2) + n_{\text{pl}}^2 \omega^2}$ is the typical length scale of graviton-photon mixing oscillations.

Regarding the general case with a spatial varying magnetic field distributed along the path of the GW propagation, the non-commutativity of $[K(l), K(l')] \neq 0$ prevents us from expressing $\mathcal{U}(l, l_0)$ in an exponential form as the case of constant magnetic field. Since the cosmic magnetic field is expected to be significantly suppressed due to the high isotropy and homogeneity of our Universe, the coupling between the graviton-photon mixing system and

the external magnetic field can be treated as a perturbative interaction. We follow the same perturbative approach in Refs. [7, 31, 36, 37, 41] and split $K(l)$ as $K(l) = K_0 + \delta K(l)$ with

$$K_0 = \begin{pmatrix} \omega & 0 & 0 & 0 \\ 0 & \omega & 0 & 0 \\ 0 & 0 & \omega(n_{\text{pl}} + 1) & 0 \\ 0 & 0 & 0 & \omega(n_{\text{pl}} + 1) \end{pmatrix}, \delta K(l) = \begin{pmatrix} 0 & 0 & -i\frac{1}{2}\kappa\mathbf{B}_x & i\frac{1}{2}\kappa\mathbf{B}_y \\ 0 & 0 & i\frac{1}{2}\kappa\mathbf{B}_y & i\frac{1}{2}\kappa\mathbf{B}_x \\ i\frac{1}{2}\kappa\mathbf{B}_x & -i\frac{1}{2}\kappa\mathbf{B}_y & 0 & 0 \\ -i\frac{1}{2}\kappa\mathbf{B}_y & -i\frac{1}{2}\kappa\mathbf{B}_x & 0 & 0 \end{pmatrix}. \quad (\text{II.7})$$

Physically speaking, l -independent K_0 describes the graviton-photon mixing system free of external field, whereas $\delta K(l)$ is a perturbation matrix that takes into account the interaction of system with the magnetic background. One can arrange Eq. (II.5) into $\partial_l \left(e^{-i\int_{l_0}^l dl' K_0(l')} \mathcal{U}(l, l_0) \right) = i e^{-i\int_{l_0}^l dl' K_0(l')} \delta K(l) \mathcal{U}(l, l_0)$ and iteratively solve it up to the first order

$$\mathcal{U}(l, l_0) = e^{i(l-l_0)K_0} + i e^{i(l-l_0)K_0} \int_{l_0}^l dl' e^{-i(l'-l_0)K_0} \delta K(l') e^{i(l'-l_0)K_0} + O(\delta K^2). \quad (\text{II.8})$$

Accordingly, the absolute value of terms $\mathcal{U}_{31}, \mathcal{U}_{32}, \mathcal{U}_{41}, \mathcal{U}_{42}$ can be obtained as

$$\begin{aligned} |\mathcal{U}_{31}(l, l_0)|^2 &= |\mathcal{U}_{42}(l, l_0)|^2 = \frac{1}{4}\kappa^2 \int_{l_0}^l dl_1 \int_{l_0}^{l_1} dl_2 e^{-2i(l_1-l_2)l_{\text{osc}0}^{-1}} \mathbf{B}_x(l_1) \mathbf{B}_x(l_2), \\ |\mathcal{U}_{32}(l, l_0)|^2 &= |\mathcal{U}_{41}(l, l_0)|^2 = \frac{1}{4}\kappa^2 \int_{l_0}^l dl_1 \int_{l_0}^{l_1} dl_2 e^{-2i(l_1-l_2)l_{\text{osc}0}^{-1}} \mathbf{B}_y(l_1) \mathbf{B}_y(l_2), \end{aligned} \quad (\text{II.9})$$

where $l_{\text{osc}0} = \frac{2}{|n_{\text{pl}}|\omega}$. Note that $e^{-2i(l_1-l_2)l_{\text{osc}0}^{-1}}$ is the same for above all four \mathcal{U} components due to the negligence of the polarization difference. The parameters of interests are $B \lesssim 10^{-9}$ Gauss and $\omega \gtrsim 10^6$ Hz, thus an order-of-magnitude estimations show that $\kappa B \lesssim 10^{-31}\text{m}^{-1}$ and $10^{-22}\text{m}^{-1} \lesssim |n_{\text{pl}}|\omega \lesssim 10^{-13}\text{m}^{-1}$. It means that magnetic term can be safely neglected so that expression $l_{\text{osc}} = 2/\sqrt{\kappa^2(\mathbf{B}_x^2 + \mathbf{B}_y^2) + n_{\text{pl}}^2\omega^2}$ reduces to $l_{\text{osc}0} = 2/(|n_{\text{pl}}|\omega)$. In this way, we consistently use the same symbol l_{osc} throughout the paper.

Let us consider a stochastic magnetic field generated in the primordial Universe. The primordial magnetic field is typically modelled as a statistically isotropic Gaussian distributed random field with a vanishing average expectation $\langle \mathbf{B}_i(\mathbf{x}) \rangle = 0$ but a non-vanishing correlation function [23] as

$$\langle \mathbf{B}_i(\mathbf{x}) \mathbf{B}_j(\mathbf{x}') \rangle = \frac{1}{(2\pi)^3} \int d^3k e^{i\mathbf{k}\cdot(\mathbf{x}'-\mathbf{x})} \left[\left(\delta_{ij} - \hat{\mathbf{k}}_i \hat{\mathbf{k}}_j \right) P_B(k) - i\epsilon_{ijm} \hat{\mathbf{k}}_m P_{aB}(k) \right], \quad (\text{II.10})$$

where $\hat{\mathbf{k}} = \mathbf{k}/k$ and ϵ_{ijm} is the totally antisymmetric symbol. The $P_B(k)$ and $P_{aB}(k)$ are the symmetric and antisymmetric parts of the power spectrum. For a given field configuration, the total magnetic energy density is $\rho_B = \langle \mathbf{B}^2(\mathbf{x}) \rangle / 2 = \int dk k^2 P_B(k) / (2\pi^2)$, the energy density per unit and per logarithm k -interval are $d\rho_B/dk = \rho_B(k) = k^2 P_B(k) / (2\pi^2)$ and $d\rho_B/d\ln k = k^3 P_B(k) / (2\pi^2)$ respectively. The root mean square $B \equiv \sqrt{\langle \mathbf{B}^2(\mathbf{x}) \rangle}$, is used as a measure of the average strength of the magnetic field. Moreover, the field strength smoothed over a certain region of size λ corresponds to $B_\lambda = \frac{8\pi}{\lambda^3} P_B(2\pi/\lambda)$. The coherence length of stochastic magnetic field is given by $\lambda_B = 2\pi \rho_B^{-1} \int \rho_B(k) k^{-1} dk$ and the corresponding strength density is $B_{\lambda_B} = \frac{8\pi}{\lambda_B^3} P_B(2\pi/\lambda_B)$. In general, λ_B represents the scale at which most of the power energy is concentrated (except the very red spectrum like the scale invariant one), thus B_{λ_B} can be used to normalize the power spectrum $P_B(k)$. Alternatively, the root mean square B can also be used to normalize $P_B(k)$. These two normalization approaches lead to similar results with a slightly difference by an order of one.

From Eq. (II.10), one can extract the transverse part

$$\langle \mathbf{B}_x(l) \mathbf{B}_x(l') + \mathbf{B}_y(l) \mathbf{B}_y(l') \rangle = \frac{1}{(2\pi)^3} \int d^3k e^{ik \cos \theta (l'-l)} (1 + \cos^2 \theta) P_B(k), \quad (\text{II.11})$$

where $\hat{\mathbf{k}}_x \hat{\mathbf{k}}_x + \hat{\mathbf{k}}_y \hat{\mathbf{k}}_y + \hat{\mathbf{k}}_z \hat{\mathbf{k}}_z = 1$ is used. Here θ denotes the angle between wave-vector \mathbf{k} of the external magnetic field and the l -direction of GW propagation. Substituting Eqs. (II.9) and (II.11) into Eq. (II.4), we average the conversion probability over all possible magnetic field configurations and obtain the main formula in this paper:

$$\begin{aligned} \langle \mathcal{P}(\Delta l) \rangle &= \frac{1}{4} \kappa^2 \int_{l_0}^l dl_1 \int_{l_0}^{l_1} dl_2 e^{-2i(l_1-l_2)l_{\text{osc}}^{-1}} \langle \mathbf{B}_x(l_1) \mathbf{B}_x(l_2) + \mathbf{B}_y(l_1) \mathbf{B}_y(l_2) \rangle \\ &= \frac{\kappa^2}{8\pi^2} \int \frac{1}{k} P_B(k) dk \left\{ 2k + \frac{1}{\Delta l} (\sin((2l_{\text{osc}}^{-1} - k) \Delta l) - \sin((2l_{\text{osc}}^{-1} + k) \Delta l)) \right. \\ &\quad + 2 \frac{4l_{\text{osc}}^{-2} + k^2}{2l_{\text{osc}}^{-1} - k} \sin^2 \left(\frac{1}{2} (2l_{\text{osc}}^{-1} - k) \Delta l \right) - 2 \frac{4l_{\text{osc}}^{-2} + k^2}{2l_{\text{osc}}^{-1} + k} \sin^2 \left(\frac{1}{2} (2l_{\text{osc}}^{-1} + k) \Delta l \right) \\ &\quad + 4l_{\text{osc}}^{-1} \left(\text{Ci}(|(2l_{\text{osc}}^{-1} + k) \Delta l|) - \text{Ci}(|(2l_{\text{osc}}^{-1} - k) \Delta l|) + \ln \left| \frac{2l_{\text{osc}}^{-1} - k}{2l_{\text{osc}}^{-1} + k} \right| \right) \\ &\quad \left. + \Delta l (4l_{\text{osc}}^{-2} + k^2) (\text{Si}((2l_{\text{osc}}^{-1} + k) \Delta l) - \text{Si}((2l_{\text{osc}}^{-1} - k) \Delta l)) \right\}, \end{aligned} \quad (\text{II.12})$$

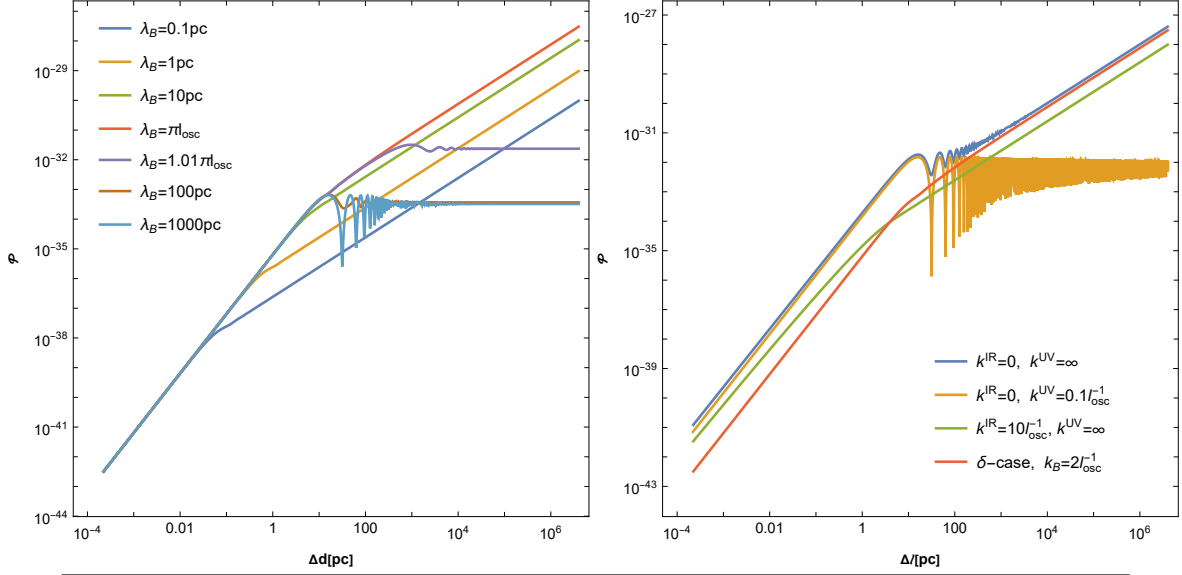
where $\text{Ci}(x) = -\int_x^\infty \frac{\cos(x')}{x'} dx'$ and $\text{Si}(x) = \int_0^x \frac{\sin(x')}{x'} dx'$. In the second equality we have used $\int_{l_0}^l dl' \int_{l_0}^{l'} dl'' e^{i2\alpha(l''-l')} = \frac{1}{\alpha^2} \sin^2(\alpha(l-l_0))$. It should be pointed out that $k = 2l_{\text{osc}}^{-1}$ is not a singularity. Moreover, the integral remains finite because of the existence of physical infrared and ultraviolet cutoffs of $P_B(k)$.

III. RESONANCE

In last section we derived a general expression, Eq. (II.12), to calculate the probability of a graviton transition to a photon in a stochastic magnetic background with spectrum $P_B(k)$. In order to explore the dependence of conversion probability to traveling distance, oscillation length and magnetic spectrum, let us first consider the magnetic spectrum as monochromatic-like. Specifically, we parametrize the power spectrum as

$$P_B(k) = \pi^2 B^2 \delta(k - k_B) / k_B^2 \quad (\text{III.13})$$

with $k_B = 2\pi/\lambda_B$. It corresponds to $d\rho/d\ln k = B^2 \delta(k/k_B - 1)/2$, which implies that all the energy is stored at a plane wave with a certain wave-number k_B . In this specific case, Eq. (II.12) can be simplified. After performing a straightforward calculation, we find that at sufficiently short distance, the probability behaves as $\mathcal{P} \simeq \kappa^2 B^2 \Delta l^2$. At large distance, the behaviour around $k_B = 2l_{\text{osc}}^{-1}$, corresponding to $\lambda_B = \pi l_{\text{osc}}$, plays a leading role. The last term in the bracket in Eq. (II.12) is the most relevant, corresponding to $\mathcal{P} \simeq \Delta l (4l_{\text{osc}}^{-2} + k_B^2) (\text{Si}((2l_{\text{osc}}^{-1} + k_B) \Delta l) - \text{Si}((2l_{\text{osc}}^{-1} - k_B) \Delta l))$. For $k_B < 2l_{\text{osc}}^{-1}$, i.e. $\lambda_B > \pi l_{\text{osc}}$, this term does not diverge and thus the entire expression converges to a finite value $\mathcal{P} \simeq \kappa^2 B^2 l_{\text{osc}}^2$ for large enough Δl and λ_B . Whereas $k_B \geq 2l_{\text{osc}}^{-1}$, i.e. $\lambda_B \leq \pi l_{\text{osc}}$, this term is proportional to the Δl and dominates over other terms, leading to an enhanced probability $\mathcal{P} \simeq \kappa^2 B^2 \lambda_B \Delta l$ at large distance. Such an amplification effect is of particular interest. In order to visualize this effect more clearly, we set $l_{\text{osc}} = 10\text{pc}$ and $B = 10^{-12}\text{Gauss}$ and we plot the conversion probability as a function of Δl with different λ_B in the upper-left panel of Fig. 1. In the case with $\lambda_B \gtrsim \mathcal{O}(10)l_{\text{osc}}$, the probability curve first grows as $\mathcal{P} \propto \Delta l^2$ at short distance $\Delta l < l_{\text{osc}}$, then it oscillates at $\Delta l \simeq l_{\text{osc}}$ and finally it reaches a plateau at $\mathcal{P} \simeq \kappa^2 B^2 l_{\text{osc}}^2$ when Δl is sufficiently large. On the other hand, when $\lambda_B \leq \pi l_{\text{osc}}$, the probability curve behaves similarly to the previous case at short distance $\Delta l \lesssim \lambda_B$, but it increases linearly at $\Delta l \gtrsim \lambda_B$ besides reaching a constant value. Such a linear amplification becomes strongest when a critical equality condition $\lambda_B = \pi l_{\text{osc}}$ is satisfied (the red line in upper-left panel in Fig. 1). It is worth mentioning that a similar linear resonance effect has been observed in previous works [7, 38, 40]. In particular, in Ref. [40] the authors worked in the context of electron density perturbation; in Ref. [38] this linear relation between probability and distance was found in the $\lambda_B \ll l_{\text{osc}}$ case; we will discuss Ref. [7] in more detail in the next section.



monochromatic power spectrum	$\lambda_B > l_{osc}$	$\Delta l \gtrsim l_{osc}$	$\Delta l < l_{osc}$
		$\mathcal{P} \simeq \kappa^2 B^2 l_{osc}^2$	$\mathcal{P} \simeq \kappa^2 B^2 \Delta l^2$
	$\lambda_B \lesssim l_{osc}$	$\Delta l \gtrsim \lambda_B$	$\Delta l < \lambda_B$
		$\mathcal{P} \simeq \kappa^2 B^2 \lambda_B \Delta l$	$\mathcal{P} \simeq \kappa^2 B^2 \Delta l^2$
scale invariant power spectrum	$k^{IR} \lesssim l_{osc}^{-1} \lesssim k^{UV}$	$\Delta l \gtrsim l_{osc}$	$\Delta l < l_{osc}$
		$\mathcal{P} \simeq \kappa^2 B^2 l_{osc} \Delta l$	$\mathcal{P} \simeq \kappa^2 B^2 \Delta l^2$
	$l_{osc}^{-1} < k^{IR} < k^{UV}$	$\Delta l \gtrsim 1/k^{IR}$	$\Delta l < 1/k^{IR}$
		$\mathcal{P} \simeq \kappa^2 B^2 \Delta l / k^{IR}$	$\mathcal{P} \simeq \kappa^2 B^2 \Delta l^2$
	$k^{IR} < k^{UV} < l_{osc}^{-1}$	$\Delta l \gtrsim l_{osc}$	$\Delta l < l_{osc}$
		$\mathcal{P} \simeq \kappa^2 B^2 l_{osc}^2$	$\mathcal{P} \simeq \kappa^2 B^2 \Delta l^2$

FIG. 1: Upper: the conversion probability from graviton to photon in the presence of the stochastic magnetic field with the monochromatic (Left) and scale invariant (Right) power spectra. The characteristic oscillation length of graviton-photon mixing is chosen to be $l_{osc} = 10\text{pc}$ and the strength of the magnetic field is set to $B = 10^{-12}\text{Gauss}$. Lower: the pattern of conversion probability after GW traveling a distance Δl in two spectra. In upper plots, an order-of-magnitude estimation is performed focusing on envelopes of the curves. Here conventions as $a > b$, $a \simeq b$ and $a < b$ correspond to $a > \mathcal{O}(10)b$, $a \simeq \mathcal{O}(1)b$ and $a < \mathcal{O}(0.1)b$, respectively.

By using the monochromatic power spectrum $P_B \sim \delta(k - k_i)$ as a basis, we can approximate any form of the multi-chromatic power spectrum as $P_B \sim \sum_i \alpha_i \delta(k - k_i)$ with varying magnitudes α_i . This approach allows us to infer the behaviour of the conversion probability with a complicated power spectrum from the well-studied monochromatic case. As an illustrative example, let us consider the scale invariant power spectrum given by

$$P_B(k) = \pi^2 B^2 / k^3, \quad k^{IR} < k < k^{UV}, \quad (\text{III.14})$$

where k^{IR} and k^{UV} are the infrared and ultraviolet cutoffs, respectively. Because of scale invariance, the magnetic field strength is smoothly averaged over a region of any size λ within the cutoffs, resulting in $B_\lambda = B$. In terms of energy density, the monochromatic power spectrum Eq. (III.13) corresponds to $d\rho/d\ln k = B^2 \delta(k/k_B - 1)/2$, whereas the scale invariant one is $d\rho/d\ln k = B^2/2$ at $k^{IR} < k < k^{UV}$. Thus, the scale-invariant power spectrum can be regarded as an opposite extreme profile to the monochromatic scenario since its energy is uniformly distributed across all scales. Due to the critical point $k_B = 2l_{\text{osc}}^{-1}$, its relative position with respect to the cutoffs of scale invariant power spectrum determines the behavior of probability. Indeed, as shown in the upper-right panel of Fig. 1, the pattern of the probability curves are determined by the relative scales of l_{osc}^{-1} , k^{IR} and k^{UV} . When $k^{UV} < 2l_{\text{osc}}^{-1}$, the dependence of probability on distance is similar to the non-resonant case in monochromatic scenario. When $2l_{\text{osc}}^{-1} \leq k^{UV}$, the probability curve has a linear amplification in the large distance. For $k^{IR} \leq 2l_{\text{osc}}^{-1} \leq k^{UV}$, the probability is maximally resonant (the critical red line in Fig. 1) and becomes insensitive to the cutoffs. This can be easily understood if we roughly consider the scale invariant power spectrum as a sum $P_B \sim \sum_{k_i} \delta(k - k_i)$ with k_i quasi-continues within the cutoff: then the main contribution comes from the critical point, especially at sufficiently large distances.

In fact, the resonance effect observed above is essentially of the same origin as the resonance addressed in Ref. [36]. In Ref. [36] the authors studied a magnetic field oscillating at a certain frequency. This situation is reminiscent of the monochromatic spectrum, as the Fourier transformation of $\delta(k - k_B)$ corresponds to a plane wave $e^{ik_B l}$. However, there are remarkable differences between our case and that in Ref. [36]. In Ref. [36] the resonance only occurs at exact condition $\lambda_B = \pi l_{\text{osc}}$ and the probability scales as $\mathcal{P} \propto \Delta l^2$. In contrast, in our case the resonance occurs in remarkably broader region for all $\lambda_B \leq \pi l_{\text{osc}}$ and the probability scales as $\mathcal{P} \propto \Delta l$ (see Fig. 2). The reason for these differences lies in

the dimensional degrees of freedom of the system under study. Indeed, the magnetic model considered in Ref. [36] is a 1-dimensional system, where the oscillatory magnetic field is parameterized as $\mathbf{B}_x(l) = B\cos(k_B(l - l_0))$ and $\mathbf{B}_y = \mathbf{B}_z = 0$. Using Eqs. (II.4) and (II.9), we obtain the conversion probability

$$\langle \mathcal{P}(\Delta l) \rangle = \frac{1}{4} \kappa^2 B^2 \frac{1}{(-4l_{\text{osc}}^{-2} + k_B^2)^2} \{ 4l_{\text{osc}}^{-2} \cos^2(k_B \Delta l) + 4l_{\text{osc}}^{-2} + k_B^2 \sin^2(k_B \Delta l) - 8l_{\text{osc}}^{-2} \cos(k_B \Delta l) \cos(2l_{\text{osc}}^{-1} \Delta l) - 4l_{\text{osc}}^{-1} k_B \sin(2l_{\text{osc}}^{-1} \Delta l) \sin(k_B \Delta l) \}. \quad (\text{III.15})$$

In the critical point $k_B = 2l_{\text{osc}}^{-1}$, i.e. $\lambda_B = 2\pi/k_B = \pi l_{\text{osc}}$, the resonance is excited and the probability increases as $\mathcal{P}(\Delta l) \propto \Delta l^2$. In our model, the magnetic vector randomly points in different direction in 3D spatial space. In mathematical terms, this introduces a misalignment between the magnetic vector direction and the GW propagation direction, represented by the angle θ in $e^{i(2l_{\text{osc}}^{-1} - k \cos \theta)(l'' - l')}$ in Eq. (II.12). Consequently, the critical point becomes $k \cos \theta \simeq l_{\text{osc}}^{-1}$, resulting in a broader resonance region at $\lambda_B \lesssim l_{\text{osc}}$. In physical picture, the resonance with $\lambda'_B \lesssim l_{\text{osc}}$ towards the GW propagation direction can be viewed as a projection of the resonance with $\lambda_B \simeq l_{\text{osc}}$ in another direction, where the angle between these two directions is θ and $\lambda'_B = \lambda_B \cos \theta$.

IV. DISCRETIZATION SCHEME

In the previous section, we showed that the probability of graviton conversion to photon can be resonantly amplified with linear growth, in limit of large propagation distance. However, an extremely long duration of the resonance is unlikely to happen in realistic situations due to several decoherence factors, e.g. the inhomogeneity of the electron density. Accordingly, an appropriate discretization scheme to make a division along the line of sight is demanded. In our case, the main source of decoherence arises from the expansion of the Universe. The graviton-photon mixing system described by Eq. (II.1) is in Minkowski space-time. In order to incorporate the expansion of the Universe, we now work in the comoving frame by replacing ∂_t with $\frac{1}{a} \partial_t$ in Eq. (II.1). Moreover, we focus on the conversion process of mixing system during the Post-Recombination era. Thus, we can still use the arguments as mentioned in above Eq. (II.3) to reasonably neglect the Cotton-Mouton effect as well as Faraday Rotation when relevant quantities are properly scaled. Therefore the modified

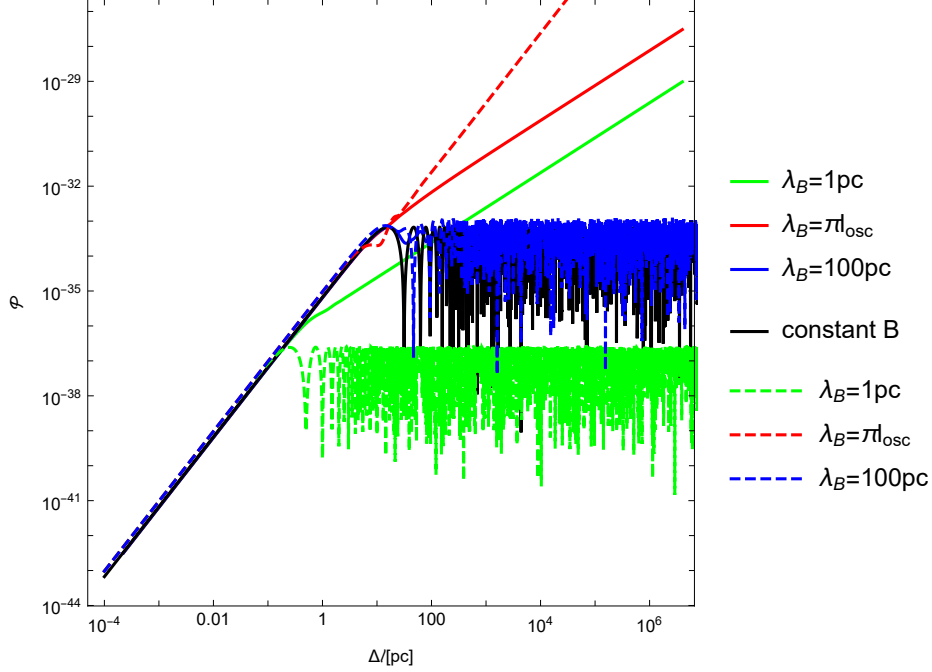


FIG. 2: The conversion probability in different representative cases. The parameters are chosen as $l_{\text{osc}} = 10\text{pc}$ and $B = 10^{-12}\text{Gauss}$. The black line denotes the case with constant magnetic field (Eq. (II.6) with $B = \sqrt{\mathbf{B}_x + \mathbf{B}_y}$). The green, red and blue solid lines represent the monochromatic spectrum of the stochastic magnetic field with different coherent lengths λ_B (Eq. (II.12)). The dashed lines represent the oscillatory magnetic field in certain wavelengths displayed in caption (Eq. (III.15) with $B = \mathbf{B}_x$).

equation reads as follows: $\partial_l(h_\times, h_+, A_x, A_y)^T = iK(a, l)(h_\times, h_+, A_x, A_y)^T$ with

$$K(a, l) = a \begin{pmatrix} \omega(a) & 0 & -i\frac{1}{2}\kappa\mathbf{B}_x(a) & i\frac{1}{2}\kappa\mathbf{B}_y(a) \\ 0 & \omega(a) & i\frac{1}{2}\kappa\mathbf{B}_y(a) & i\frac{1}{2}\kappa\mathbf{B}_x(a) \\ i\frac{1}{2}\kappa\mathbf{B}_x(a) & -i\frac{1}{2}\kappa\mathbf{B}_y(a) & \omega(a)(n_{\text{pl}}(a) + 1) & 0 \\ -i\frac{1}{2}\kappa\mathbf{B}_y(a) & -i\frac{1}{2}\kappa\mathbf{B}_x(a) & 0 & \omega(a)(n_{\text{pl}}(a) + 1) \end{pmatrix}, \quad (\text{IV.16})$$

where a denotes the scaling factor and l the comoving distance. Here, quantities are scaled as $\omega(a) = \omega_0/a$, $\mathbf{B}_x(a, l) = \mathbf{B}_{x0}(l)/a^2$, $\mathbf{B}_y(a, l) = \mathbf{B}_{y0}(l)/a^2$ and $n_{\text{pl}}(a) = -e^2 n_{b0} X_e(a) / (2a\omega_0^2 m_e)$, where the subscript 0 denotes the corresponding value at present day, $n_{b0} \simeq 0.25\text{m}^{-3}$ is the baryon number density today and $X_e(a)$ is the ionization fraction. We consider the magnetic field as diluted by the expansion of the Universe, neglecting its dynamical evolution [23]. Additionally, we sharpen the parameterization as $X_e(a) \simeq 10^{-4}$ ($0.002 \lesssim a \lesssim 0.05$) and otherwise $X_e(a) \simeq 1$ [44]. As we will see later, this simplification is

enough accurate for our purposes.

Let us note that the non-commutativity of $K(a)$ at different cosmic time renders searches of solutions for Eq. (IV.16) more difficult than previous cases studied above. Therefore, we consider a steady approximation as follows. We consider an interval of cosmic time during which the relative change of K due to the Universe expansion has to be small enough, allowing us to approximate the equation with a constant K scaled at that specific time. Physically, this approximation means that the GW does not “feel” the expansion of Universe when it propagates during such a short time interval. We stress that one can not take the interval infinitely small, otherwise the coherence of the system would be lost and hence the total conversion probability along the line of sight would vanish. In order to determine the appropriate time interval, we examine how K changes with respect to the conformal time τ . We only need to concern about the first three components of K those scales as $1/a$. During a time interval $\Delta\tau$, for example for the first component, it relatively changes as $\Delta K_{11}/K_{11} = \mathcal{H}\Delta\tau$, by using $d(1/a)/d\tau = \mathcal{H}/a$ with the comoving Hubble parameter \mathcal{H} . The steady approximation demands that relative change $\epsilon = \Delta K_{11}/K_{11}$ is small all the time. Regarding the comoving distance Δl , this requirement can be translated into $\Delta l = \Delta\tau = \epsilon\mathcal{H}^{-1}$. This means that the GW traveling distance is a small portion of the comoving Hubble radius \mathcal{H}^{-1} . This makes sense because the Hubble radius characterizes the size of the local inertial frame in the expanding Universe. In other words, the graviton-photon mixing system does not strongly "feel" the Universe expansion in a suitable interval of cosmic time. A similar approximation has also been considered for axion-photon mixing in expanding Universe [43].

In terms of the redshift $z = 1/(1+a)$, the steady approximation leads to a discretization scheme by setting a redshift sequence $[z_1, z_2, \dots, z_N]$ iterated via $z_{n+1} = (1 - \epsilon)z_n$ ($n = 1, 2, \dots, N - 1$). Since we consider the primordial magnetic field at the Post-Recombination era, the initial point is set to the end of Recombination $z_1 \simeq 1100$ and the iteration continues until the present day. The comoving distance Δl_n of GW path during interval patch $[z_n, z_{n+1}]$ is given by $\Delta l_n = \epsilon\mathcal{H}^{-1}(z_n)$, where $\mathcal{H}(z_n) = H_0(1 + z_n)^{1/2}$ with H_0 being the Hubble parameter today. In each patch, we construct the kernel matrix $K(z, x)$ with values evaluated at $z = z_n$ in Eq. (IV.16) and perform the same perturbative approach as the Minkowski

spacetime case. Thus, we obtain:

$$\langle \mathcal{P}(\Delta l, z_n) \rangle = \frac{1}{(1+z_n)^2} \frac{1}{4} \kappa^2 \int_{l_0}^l dl' \int_{l_0}^{l'} dl'' e^{-2i(l'-l'')l_{\text{osc}}^{-1}(z_n)} \langle \mathbf{B}_x(z_n, l') \mathbf{B}_x(z_n, l'') + \mathbf{B}_y(z_n, l') \mathbf{B}_y(z_n, l'') \rangle, \quad (\text{IV.17})$$

where $l_{\text{osc}}(z_n) = 2(1+z_n)/(|n_{\text{pl}}|\omega)$ is the comoving oscillation length. Here we use the same symbol l_{osc} as clearly understood in both the static and expanding cases. To derive Eq. (IV.17), we have used Eq. (II.4) which is correct only when the initial GW mode is unpolarized. In fact, the GW can be perfectly regarded as an unpolarized source during the whole Post-Recombination era because of the suppressed conversion probability from GW to photon even in the occurrence of the resonance (typically $< 10^{-10}$, as we will see later). Finally, we obtain the conversion probability during interval patch $[z_n, z_{n+1}]$ under the expansion of universe as

$$\begin{aligned} \langle \mathcal{P}^{\text{exp}}(\Delta l_n) \rangle &= \frac{1}{(1+z_n)^2} \frac{\kappa^2}{8\pi^2} \int \frac{1}{k} P_B(z_n, k) dk \left\{ 2k + \frac{1}{\Delta l_n} (\sin((2l_{\text{osc}}^{-1} - k) \Delta l_n) - \sin((2l_{\text{osc}}^{-1} + k) \Delta l_n)) \right. \\ &\quad + 2 \frac{4l_{\text{osc}}^{-2} + k^2}{2l_{\text{osc}}^{-1} - k} \sin^2\left(\frac{1}{2}(2l_{\text{osc}}^{-1} - k) \Delta l_n\right) - 2 \frac{4l_{\text{osc}}^{-2} + k^2}{2l_{\text{osc}}^{-1} + k} \sin^2\left(\frac{1}{2}(2l_{\text{osc}}^{-1} + k) \Delta l_n\right) \\ &\quad + 4l_{\text{osc}}^{-1} \left(\text{Ci}(|(2l_{\text{osc}}^{-1} + k) \Delta l_n|) - \text{Ci}(|(2l_{\text{osc}}^{-1} - k) \Delta l_n|) + \ln \left| \frac{2l_{\text{osc}}^{-1} - k}{2l_{\text{osc}}^{-1} + k} \right| \right) \\ &\quad \left. + \Delta l_n (4l_{\text{osc}}^{-2} + k^2) (\text{Si}((2l_{\text{osc}}^{-1} + k) \Delta l_n) - \text{Si}((2l_{\text{osc}}^{-1} - k) \Delta l_n)) \right\}. \end{aligned} \quad (\text{IV.18})$$

Here the magnetic field spectrum $P_B(z_n, k)$ is defined in the same formula as in Eq. (II.10) but with respect to the time-dependent correlation function $\langle \mathbf{B}_i(z_n, \mathbf{x}) \mathbf{B}_j(z_n, \mathbf{x}') \rangle$. The total conversion probability along the line of sight is given by adding all probability contributions from all patches, namely $\mathcal{P}_{\text{total}} = \sum_{n=1}^{N-1} \mathcal{P}^{\text{exp}}(\Delta l_n)$.

In order to justify the aforementioned assumption of simplified parameterization of ionization fraction $X_e(z)$, we show the oscillation length $l_{\text{osc}}(z)$ and conversion probability $\mathcal{P}^{\text{exp}}(\Delta l_n)$ as a function of redshift in Fig. 3. As shown in this Figure, a step-like approximation of $X_e(z)$ does not relevantly change the main results. Moreover, this also shows that the conversion probability can be safely neglected during the reionization era. The oscillation length l_{osc} reaches its maximum value before the reionization at $z \simeq 20$, indicating that the corresponding conversion probability is expected to be at its peak before reionization as well. However, due to the expansion of the universe, the Eq. (IV.18) includes an extra $(1+z)^2$ factor, which leads to a relative increase in the probability at large redshifts. Nevertheless, during the Dark Age $20 \lesssim z \lesssim 1000$, the relative changes of $l_{\text{osc}}(z)$ as well as $\mathcal{P}^{\text{exp}}(\Delta l_n)$ remains within $\mathcal{O}(10)$. Therefore, using relevant quantities at $z = 20$ is sufficient

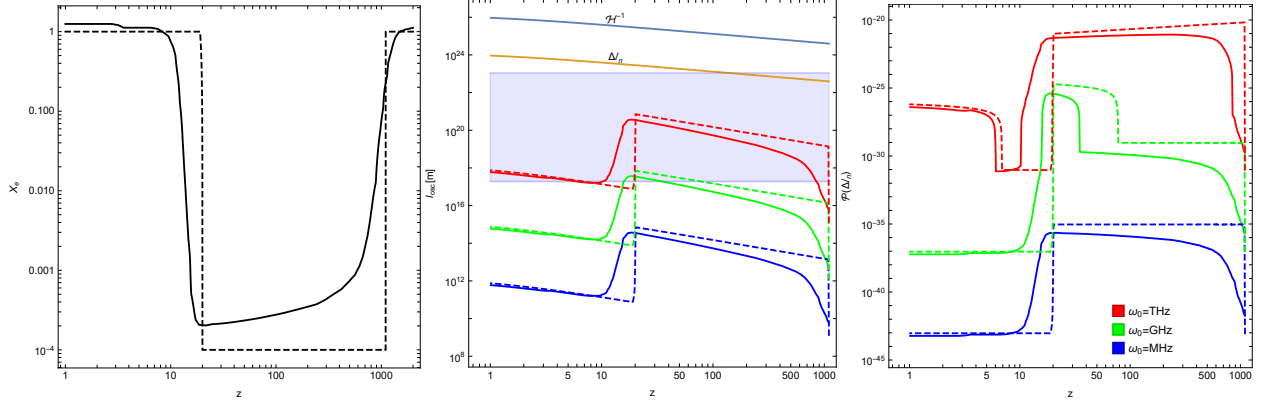


FIG. 3: Ionization fraction X_e , oscillation probability l_{osc} and conversion probability versus the redshift in the Post-Recombination era. The blue, green, red lines denote the different frequency cases with $\omega_0 = 10^6$, 10^9 and 10^{12} Hz, respectively. The solid line denotes an accurate parameterization of ionization fraction function [44], whereas the dashed line denotes the simplified parameterization in step shape. In the right panel, we show the conversion probability $\mathcal{P}(\Delta l_n)$ at each redshift interval $[z_n, z_{n+1}]$ with $\epsilon = 0.01$. Here we parameterize the magnetic field spectrum Eq. (IV.19) with $n_L = -3$, $n_S = -4$, $k^{IR} = 10^{-23}$, $k_0 = 10^{-18}$, $k_D = 10k_0$ and A is normalized to the root mean square strength $B = 10^{-12}$ Gauss. The shaded region in the middle panel is bounded by $(2/k_D, 2/k^{IR})$.

to perform order-of-magnitude analysis. In addition, the steep increase of the probability curve at $20 \lesssim z \lesssim 30$ for the case $\omega_0 = \text{GHz}$ is caused by the resonance when the condition $1/k_D \lesssim l_{osc} \lesssim 1/k^{IR}$ is satisfied (compare the green line and the shade region).

The last ingredient yet to be addressed in Eq. (IV.18) is the power spectrum of stochastic magnetic field in the expanding Universe. As mentioned in Introduction, cosmological phase transition and inflation magnetogenesis are two main hypothetical mechanisms to explain the generation of the magnetic field in the primordial universe [23, 45]. In the case of cosmological phase transition, the magnetic field is produced by bubbles coalescence in a first order phase transition. This process leads to a blue spectrum $P_B \sim k^2$ as a consequence of causality. On the other hand, inflation magnetogenesis usually leads to a blue spectrum $P_B \sim k$. To obtain a scale-invariant spectrum $P_B \sim k^{-3}$ during inflation, the inflaton has to be strongly coupled with vector fields and back-reactions are not negligible [46]. Nevertheless, several possible ways to solve these problems have been explored in Ref. [24] and reference therein.

In the Post-Recombination era, we consider an evolving magnetic field with the power spectrum that can be modelled as two power laws [47, 48]:

$$P_B(z, k) = (1+z)^4 P_{B_0}(k) = (1+z)^4 \begin{cases} A(k/k_0)^{n_L} & k^{IR} < k \leq k_0, \\ A(k/k_0)^{n_S} & k_0 < k < k_D, \end{cases} \quad (\text{IV.19})$$

where $P_{B_0}(k)$ is defined with respect to $B_0(x)$ in the comoving frame as Eq. (II.10). Here, the n_L is spectral index at large length scale encoding informations about the magnetogenesis mechanism. We focus on two representative cases with $n_L = 2$ and $n_L = -3$, corresponding to phase transition and inflation magnetogenesis, respectively. For $n_L = 2$ case, the infrared cutoff k^{IR} is normally set to the Hubble radius at the phase transition time. One can safely take k^{IR} to a infinite small value in practice since most of the power spectrum accumulates towards k_0 . Whereas for $n_L = -3$ case, k^{IR} can be interpreted as the scale when magnetogenesis starts during inflation [47]. Its value could cover a large range either being larger or smaller than the current Hubble radius. On the other hand, at small scale the field is processed by magnetohydrodynamic turbulence, leading to a universal Kolmogorov slope $n_S = -11/3$. Here we introduce a weak turbulence with $n_S = -4$ as a different MHD spectrum would only change the result by a numerical factor of order unity. At smaller scale the spectral energy is damped away via the viscosity of charged plasma during recombination, which is characterized by the ultraviolet cutoff $k_D \simeq \mathcal{O}(100)(10^{-9}\text{Gauss}/B_0)\text{Mpc}^{-1}$ [49, 50]. This cutoff defines a characteristic damping scale $\lambda_D \equiv 2\pi/k_D$. In addition, the factor A is normalized by B_0 .

V. NUMERICAL RESULTS

In this section we consider Eq. (IV.18) and the aforementioned discretization scheme. We will show numerical results of the total conversion probability as the GWs travel through the Post-Recombination era in the expanding Universe. The GWs in the ultrahigh frequency window $\omega_0 \geq \text{MHz}$ are of particular interests: they could be potentially probed in radio channel through GW-photon conversion processes. Therefore, we consider four typical frequency windows of GW $\omega_0 = 10^6\text{Hz}$, 10^9Hz , 10^{12}Hz and 10^{15}Hz and we study graviton-photon transitions in presence of the primordial magnetic background field. The results are shown in Fig. 4. The gray region in B_0 - λ_B parameter plane is ruled out by CMB analysis

and the magnetohydrodynamic turbulence [23]. Relic fields, lower than the limit from Blazar observations (the light gray zone), can not be directly tested since they can be hidden by background from other dominant EM sources. As elaborated in Ref. [23], the evolution of the magnetic field generated during Electroweak or QCD phase transition undergoes to the MHD process and it stops at the narrow blue region of parameters corresponding to Universe today. Note that we ignore the reionization era which negligibly contributes to the total probability. In contrast, the hypothetical scale invariant magnetic field generated during inflation is more interesting from the observational perspective because it could in principle be within the entire allowed observable region. Before discussing them separately, we briefly introduce two characteristic scales. One is the scale of the patch size $\Delta l_n \simeq \mathcal{O}(1 - 10)\text{Mpc}$ along the line of sight (the green shaded region in Fig. 4). The other is the oscillation length $l_{\text{osc}}(z_n)$ of graviton-photon mixing, which varies in the expanding Universe. Since the total conversion probability receives the main contribution when the oscillation length is at its maximum scale (see Fig. 3), we refer to it as l_{osc} in the following and label the corresponding value in the red vertical line.

For the relic magnetic field arising from phase transition, its strength and coherent length are constrained to the blue stripe region in Fig. 4. The spectrum modeled in Eq. (IV.19) has a blue scaling at small $k < k_0$ and red scaling at large $k > k_0$. Thus, the profile of the power spectrum resembles a monochromatic one, peaked around k_0 , with the coherent length at scale $\lambda_B \sim k_0^{-1}$. As a result, the resonant effect occurs when $\lambda_B \lesssim l_{\text{osc}}$ and it reaches its maximum at $\lambda_B \simeq l_{\text{osc}}$ (see the left panel in Fig. 1). Note that we perform an order-of-magnitude analysis since the spectrum is not a perfect δ -shape but has finite width around k_0 . Nevertheless, the main result of resonance can be applied yet. Indeed, in $\omega_0 = 10^{9,12,15}\text{Hz}$ cases, the conversion probability is resonantly amplified when the coherent length is comparable to the oscillation length scale (see the insets in Fig. 4).

In contrast, the scale invariant relic magnetic field from inflation is much less constrained and could fill the entire observable region. In this scenario, λ_B loses its original physical meaning because the strength of magnetic field is equally distributed over all scales. In fact, the definition $\lambda_B \sim \int k P_B(k) dk$ indicates that for the scale invariant spectrum $P_B \sim k^{-3}$, the value of λ_B is mainly determined by the infrared cutoff, namely $\lambda_B^{-1} \simeq k^{IR}$. Nonetheless, we still use λ_B for convenience for comparisons with observations. Generally, as indicated in Fig. 4, the conversion probability increases as the GWs frequency ω_0 or magnetic strength B_0 in-

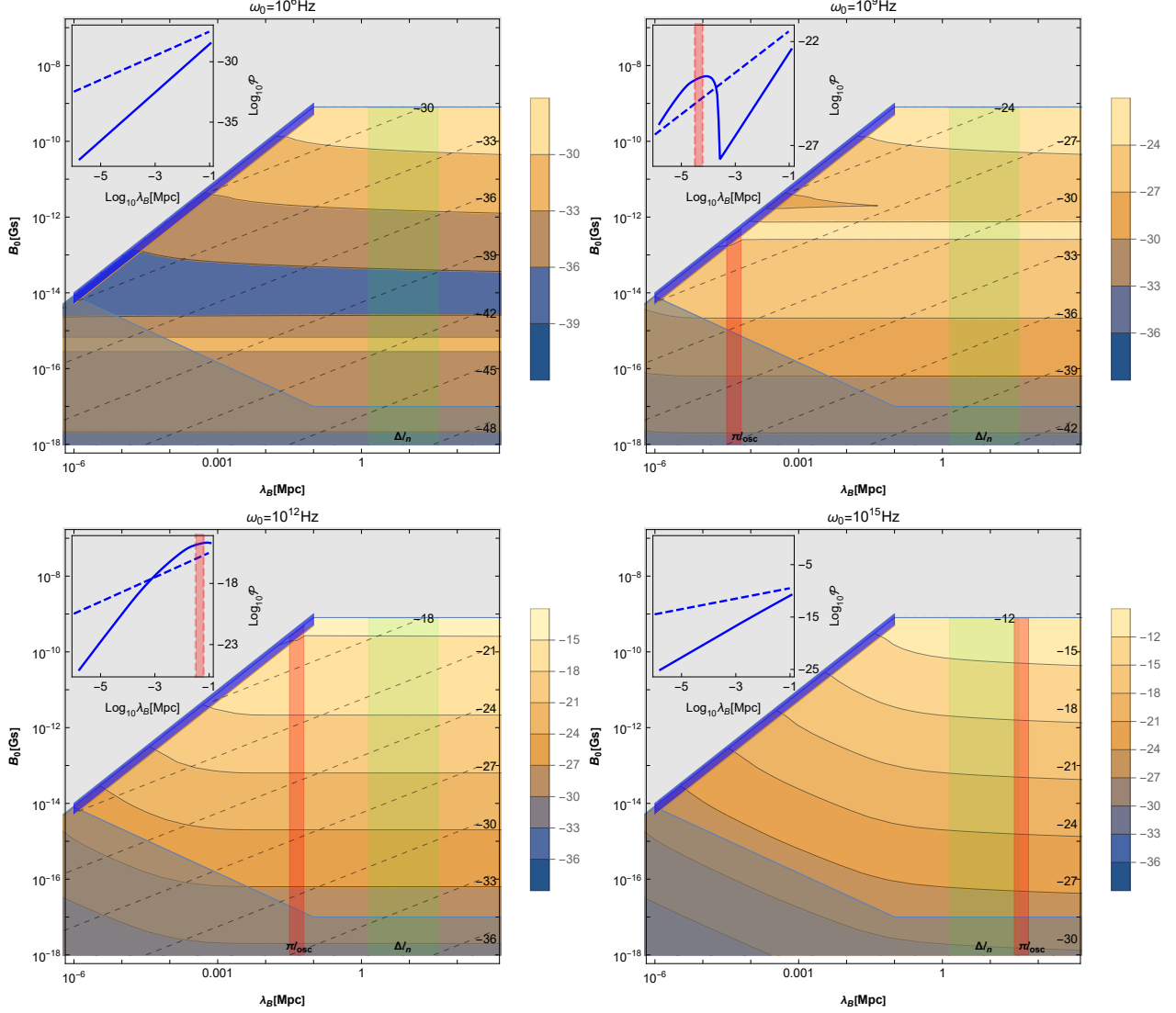


FIG. 4: The total probability $\log_{10} \mathcal{P}_{\text{total}}$ conversion from graviton with ultrahigh frequency ω_0 to photon propagating within the Post-Recombination era. The gray region shows the exclusion on the primordial magnetic relic as discussed in the text. The relic field from phase transition magnetogenesis survives at the relatively smaller coherence scale today, as shown in the narrow blue stripe region. The corresponding probability is shown in color conventions displayed in captions. The inflationary magnetogenesis can generate a scale invariant spectrum, with strength and coherence length varying in a wide range. It could in principle fill the entire allowed observational region given proper initial conditions. The red vertical line denotes the typical oscillation length scale ($\sim 10^{-8}$ Mpc in $\omega_0 = 10^6$ Hz). The green area shows the rough scale of the patch size in steady state discretization scheme. The results in Ref. [7] are labeled in dashed lines. Here we fix $\epsilon = 0.01$.

creases. The total probability can arrive up to 10^{-12} when $\omega_0 = 10^{15}\text{Hz}$ and $B_0 \sim 10^{-9}\text{Gauss}$. Such a sizable conversion probability could have detectable cosmological implications which deserve for future dedicated studies. For a fixed strength of magnetic field, the probability is insensitive to the coherent length in relatively low frequency cases with $\omega_0 = 10^6\text{Hz}$ and $\omega_0 = 10^9\text{Hz}$. In relatively high frequency cases with $\omega_0 = 10^{12}\text{Hz}$ and $\omega_0 = 10^{15}\text{Hz}$, the probability increases with a larger coherence length of the magnetic field. Regarding the resonance effect, the analysis in Sec. III reveals that the resonance is excited when the damping scale is comparable or smaller than the oscillation length, i.e. $\lambda_D \lesssim l_{\text{osc}}$ (see the upper-right panel in Fig. 1). In Fig. 4, one can observe that the conversion probability generally decreases as the strength of the magnetic field decreases. However, in $\omega_0 = 10^6\text{Hz}$ and $\omega_0 = 10^9\text{Hz}$ cases, the probability significantly increases by more than about $3 \sim 6$ orders of magnitude when the resonance condition $\lambda_D \lesssim l_{\text{osc}}$ is satisfied. Moreover, the probability is maximally resonant in a large region where the condition $\lambda_D \lesssim l_{\text{osc}} \lesssim \lambda_B$ is satisfied. This results in an amplification of the probability for the relatively weaker magnetic field and the field with relatively larger coherence length.

In Tab. I, we list the patterns of the probability in different parameter regions by the order-of-magnitude analysis. Here we omit all details and we only focus on distinct features for with/without resonance. We can see that the probability for the scale invariant scenario has much richer structure than the phase transition one. Such distinct features of the probabilities can be used to probe these two magnetogenesis scenarios from early Universe.

Let us comment on the existing domain-like magnetic field model as well as its variations, which have been adopted in almost all relevant literature dealing with cosmic magnetic fields. In these models, the line-of-sight region is divided into many patches, each with a size equal to the coherence length λ_B . To realize the stochastic property of magnetic field, in each patch the magnetic field is assumed to be uniform but chosen in a random direction. This scheme provides several simplifications for probability computations and it is often sufficient to capture the main features of the system. However, this approach is somehow artificial and it violates divergence free condition of magnetic field. On the contrary, our approach is based in statistical techniques and it is more realistic and natural to describe the stochastic configuration of magnetic field. Moreover, our approach is capable of integrating any kinds of discretization scheme. It means that the size of discrete patches is not necessary identified with coherence length of magnetic field. For a useful comparison, we add the pattern of

phase transition	$\omega_0 = 10^6 \text{Hz} (\Delta l_n > l_{\text{osc}}, \Delta l_n > \lambda_B)$	$\lambda_B > l_{\text{osc}}$	$\mathcal{P}_{\text{total}} \simeq \kappa^2 B^2 l_{\text{osc}}^2 D / \Delta l_n$
	$\omega_0 = 10^9 \text{Hz} (\Delta l_n > l_{\text{osc}}, \Delta l_n > \lambda_B)$	$\lambda_B > l_{\text{osc}}$	$\mathcal{P}_{\text{total}} \simeq \kappa^2 B^2 l_{\text{osc}}^2 D / \Delta l_n$
		$\lambda_B \lesssim l_{\text{osc}}$	$\mathcal{P}_{\text{total}} \simeq \kappa^2 B^2 \lambda_B D$
	$\omega_0 = 10^{12,15} \text{Hz} (\Delta l_n > l_{\text{osc}}, \Delta l_n > \lambda_B)$	$\lambda_B \lesssim l_{\text{osc}}$	$\mathcal{P}_{\text{total}} \simeq \kappa^2 B^2 \lambda_B D$
scale invariant (inflation)	$\omega_0 = 10^6 \text{Hz} (\Delta l_n > l_{\text{osc}}, \lambda_B > l_{\text{osc}})$	$\lambda_D \lesssim l_{\text{osc}} \lesssim \lambda_B$	$\mathcal{P}_{\text{total}} \simeq \kappa^2 B^2 l_{\text{osc}} D$
		$l_{\text{osc}} < \lambda_D < \lambda_B$	$\mathcal{P}_{\text{total}} \simeq \kappa^2 B^2 l_{\text{osc}}^2 D / \Delta l_n$
	$\omega_0 = 10^9 \text{Hz} (\Delta l_n > l_{\text{osc}})$	$\lambda_D \lesssim l_{\text{osc}} \lesssim \lambda_B$	$\mathcal{P}_{\text{total}} \simeq \kappa^2 B^2 l_{\text{osc}} D$
		$\lambda_D < \lambda_B < l_{\text{osc}}$	$\mathcal{P}_{\text{total}} \simeq \kappa^2 B^2 \lambda_B D (\Delta l_n \gtrsim \lambda_B)$
			$\mathcal{P}_{\text{total}} \simeq \kappa^2 B^2 \Delta l_n D (\Delta l_n < \lambda_B)$
		$l_{\text{osc}} < \lambda_D < \lambda_B$	$\mathcal{P}_{\text{total}} \simeq \kappa^2 B^2 l_{\text{osc}}^2 D / \Delta l_n$
	$\omega_0 = 10^{12} \text{Hz} (\Delta l_n > l_{\text{osc}}, \lambda_D < l_{\text{osc}})$	$\lambda_D \lesssim l_{\text{osc}} \lesssim \lambda_B$	$\mathcal{P}_{\text{total}} \simeq \kappa^2 B^2 l_{\text{osc}} D$
		$\lambda_D < \lambda_B < l_{\text{osc}}$	$\mathcal{P}_{\text{total}} \simeq \kappa^2 B^2 \lambda_B D$
	$\omega_0 = 10^{15} \text{Hz} (\Delta l_n < l_{\text{osc}}, \lambda_D < l_{\text{osc}})$	$\lambda_D \lesssim l_{\text{osc}} \lesssim \lambda_B$	$\mathcal{P}_{\text{total}} \simeq \kappa^2 B^2 \Delta l_n D$
		$\lambda_D < \lambda_B < l_{\text{osc}}$	$\mathcal{P}_{\text{total}} \simeq \kappa^2 B^2 \lambda_B D (\Delta l_n \gtrsim \lambda_B)$
			$\mathcal{P}_{\text{total}} \simeq \kappa^2 B^2 \Delta l_n D (\Delta l_n < \lambda_B)$
	domain-like model	all $\omega_0 (\lambda_B = \Delta l_n)$	$\lambda_B > l_{\text{osc}}$
$\lambda_B \lesssim l_{\text{osc}}$			$\mathcal{P}_{\text{total}} \simeq \kappa^2 B^2 \lambda_B D$

TABLE I: All possible cases of the total conversion probability after traveling a total distance D in different parameter regions are displayed. We perform order-of-magnitude estimations (see Fig. 1). The parameter conditions (see Fig. 4) are shown in the parentheses in the second column while corresponding probabilities in the third column.

the probability derived in the domain-like model in Tab. I. We can see that the results obtained from our approach is remarkably different to ones from domain-like model due to the resonance effect and the discretization scheme. It is interesting to note that, in a particular case with $\lambda_B \simeq \Delta l_n$, the phase transition scenario in our method leads to the same result of the domain-like model. Whereas in the scale invariant scenario, when $\lambda_D \lesssim l_{\text{osc}}$ and $\lambda_B \simeq \Delta l_n > l_{\text{osc}}$ our result receives a maximal resonant contribution, which is larger than the domain-like model by a factor $\lambda_B / l_{\text{osc}}$. This factor can be as large as about 10^9 at $\omega_0 = 10^6 \text{Hz}$, 10^5 at $\omega_0 = 10^9 \text{Hz}$ and 10^2 at $\omega_0 = 10^{12} \text{Hz}$.

We stress that even if the authors of Ref. [7] also perform a perturbative approach,

their results are completely different from our ones. The conversion probabilities obtained in Ref. [7] (the Fig. 2 therein) are shown in dashed lines in Fig. 4. In Ref. [7], the conversion rate is given by $\Gamma \sim \kappa^2 B^2 l_{\text{osc}}^2 / \lambda_B$, and hence the total probability is approximated as $\mathcal{P}_{\text{total}} \simeq \Gamma D \simeq \kappa^2 B^2 l_{\text{osc}}^2 D / \lambda_B$. Therefore, the model in Ref. [7] effectively resembles a domain-like model under the condition $\lambda_B = \Delta l_n \gtrsim l_{\text{osc}}$ (see Tab. I). Furthermore, in Ref. [7] the authors applied their probability formula to impose upper bounds on the stochastic GW background derived from EDGES [17] and ARCADE 2 [16] experiments at $\omega_0 \sim 10^8 \text{Hz}$ and 10^{10}Hz , respectively. For the scale invariant case with $\omega_0 = 10^9 \text{Hz}$ in Fig. 4, we can see that the maximum probability in the entire viable parameter region is comparable to the one in Ref. [7]. However, the remarkably different distribution of the probability density indicates that in several subregions of B_0 - λ_B plane, the corresponding bounds on GWs obtained in Ref. [7] can be either overestimated or underestimated by several orders of magnitude. In other words, comparative analysis with experimental data are model-dependent and previous bounds have to be revisited in case of resonances, especially in case of scale-invariant power spectrum. For instance, at $B_0 \lesssim 10^{-12} \text{Gauss}$ or $\lambda_B \gtrsim \text{Mpc}$, the conversion probability predicted from our model is 5 \sim 10 orders larger, hence lowering the corresponding GW bounds by 2 \sim 5 orders. From the reversed perspective, radio signals could probe the magnetic field with much weaker strength or larger coherence length than previously considered

In the end, we mention that a different choice for the value of ϵ , different than 0.01 assumed above, would affect the results as setting a different discretization. Nevertheless, one can always perform similar analysis observing the pattern of the probability behaviour in different parameter regions as illustrated in Fig. 1. For any choice of ϵ , the behaviour of probability in our model would significantly differ from the one in domain-like model. In order to demonstrate the ϵ -dependence, we show three cases with $\epsilon = 0.1, 0.01$ and 0.001 in Fig. 5. The order-of-magnitude estimation in the Tab. I can be applied to these cases as well. It is worth noticing that when the resonance happens (see the THz case for instance), the total conversion probability is insensitive to the choice of ϵ . This can be easily understood because, in the linear resonance region $\mathcal{P}(\Delta l_n) \propto \Delta l_n$, the total conversion probability, after a long fixed distance D , is expected to be $\mathcal{P}_{\text{total}}(D) \simeq N \mathcal{P}(\Delta l_n) \propto D$ with $N \simeq D / \Delta l_n$ the number of patches. However, in the non-resonance region, a sensitive ϵ -dependence of result reflects the fact that the discretization scheme is crucial.

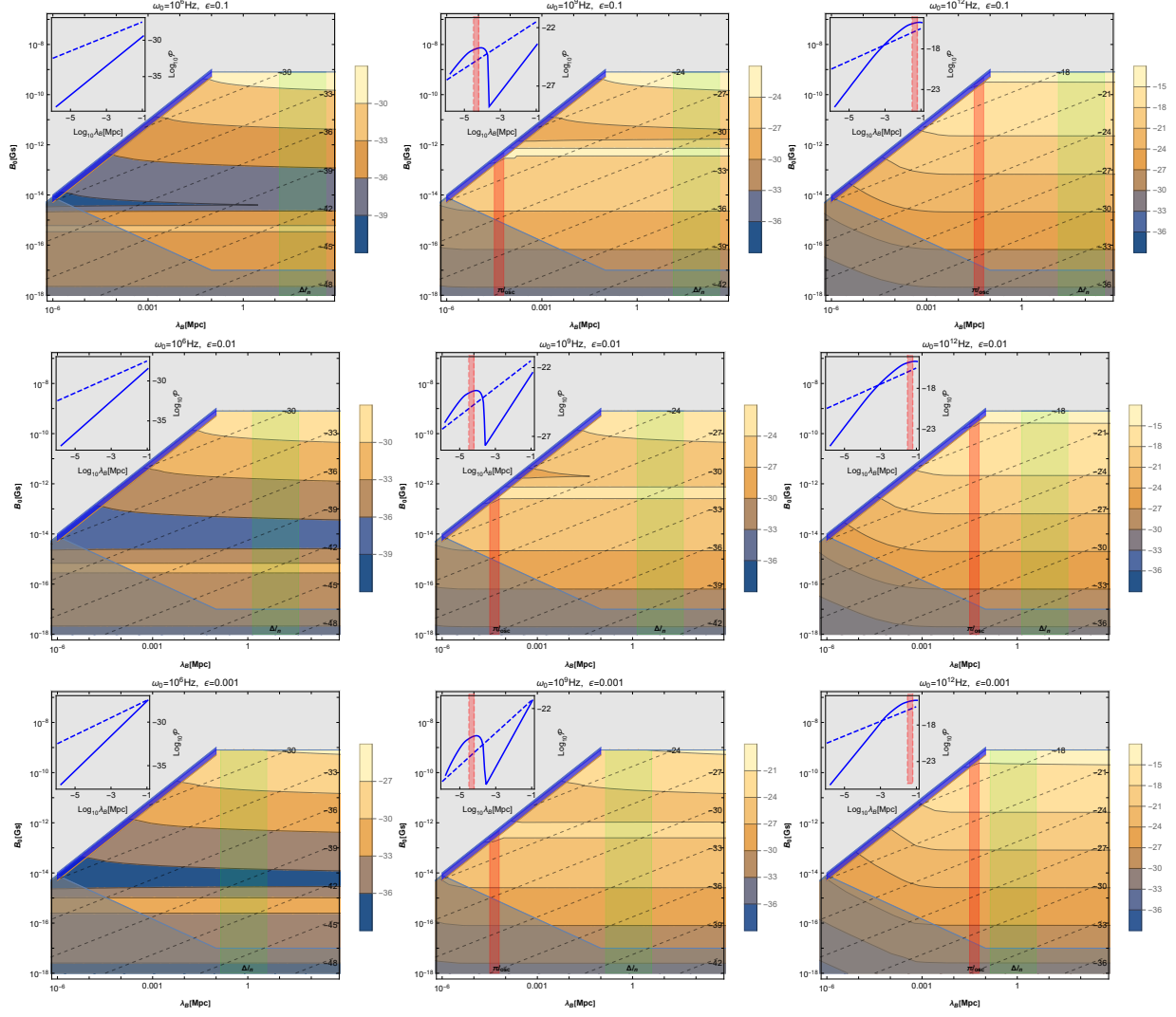


FIG. 5: The total conversion probability $\log_{10}\mathcal{P}_{\text{total}}$ in different $\epsilon = 0.1, 0.01$ and 0.001 cases. The panels in the second row with $\epsilon = 0.01$ are same to Fig. 4. The dashed lines denote the conversion probability obtained in Ref. [7].

VI. DISCUSSION AND CONCLUSIONS

In summary, our study focused on the inverse Gertsenshtein effect in a graviton-photon mixing system with an inhomogeneous stochastic magnetic background. The probability of conversion from graviton to photon can be obtained from a perturbative analysis. We found that the conversion probability can be resonantly amplified in certain parametric spaces. We first worked in the Minkowski spacetime and considered two simplified representative spectra parameterized in monochromatic and scale invariant forms. For the monochromatic

one, the resonance is obtained when the coherence length of the magnetic field λ_B becomes comparable or smaller than the oscillation length of the graviton-photon mixing l_{osc} . The resonance effect is maximally amplified at $\lambda_B \simeq l_{\text{osc}}$. On the other hand, for the scale invariant case, the resonance band lies in the region where the damping scale λ_D is comparable or smaller than l_{osc} .

Then, we included the expansion of the Universe in our analysis: cosmological acceleration enters as a decoherence factor in the transition probability. In particular, we performed a steady approximation by dividing the GW propagation distance into patches with each size corresponding to $\Delta l_n \simeq \mathcal{O}(1)\text{Mpc}$. Concerning the primordial magnetic field, we focus on the phase transition and inflation magnetogenesis. For the relic field generated from phase transition, only a narrow region in the observational B_0 - λ_B plane is allowed. We showed that the corresponding conversion probability has peak at $\lambda_B \simeq l_{\text{osc}}$ when the resonance has its max. For the scale invariant field generated during inflation, its strength and the coherence length are allowed in a large range which can fill the whole observational parameter space. In such a magnetic background, the conversion from graviton to photon is resonantly enhanced once the damping scale is smaller than the oscillation length $\lambda_D \lesssim l_{\text{osc}}$. This amplification can raise the conversion probability up to $2 \sim 5$ orders of magnitude with respect to domain-like models. Thus, the distinct features of the probability function profiles can potentially provide a way to distinguish inflation magnetogenesis from phase transitions one.

Moreover, we made a comparison between our model with the domain-like one and current experimental bounds. We found that the distribution of the probability in B_0 - λ_B plane are different to ones obtained in Ref. [7]. Thus, to include resonances leads to a revisit of GW bounds derived from EDGES and ARCADE2 experiments in Ref. [7] of several orders of magnitude, especially for small fields $B_0 \lesssim 10^{-12}\text{Gauss}$ or large coherent lengths $\lambda_B \gtrsim \text{Mpc}$. Conversely, possible radio signals can probe the cosmological magnetic field with much weaker magnetic strength or much larger coherence length.

Let us end with some short remarks. The resonance phenomenon is not exclusive to graviton-photon mixing but could manifest in other mixing systems described by Eq. (II.3) with an inhomogeneous background field, such as axion-photon mixing. Concerning the inter-galactic or intra-galactic magnetic fields in the late Universe, in principle our approach can also be applied. However, the estimation of the conversion probability strongly depends on the specific model of galactic winds, magnetization process, volume filling factor,

ionization levels and other relevant effects.

Acknowledgements.

A.A. is supported by National Science Foundation of China (NSFC) No.12350410358; the Talent Scientific Research Program of College of Physics, Sichuan University, Grant No.1082204112427 & the Fostering Program in Disciplines Possessing Novel Features for Natural Science of Sichuan University, Grant No.2020SCUNL209 & 1000 Talent program of Sichuan province 2021. S.C. acknowledges the support of Istituto Nazionale di Fisica Nucleare (INFN) (iniziative specifiche MoonLight2 and QGSKY). This paper is based upon work from the COST Action CA21136, *Addressing observational tensions in cosmology with systematics and fundamental physics* (CosmoVerse) supported by COST (European Cooperation in Science and Technology)

-
- [1] ME Gertsenshtein. Wave resonance of light and gravitational waves. *Sov Phys JETP*, 14:84–85, 1962.
 - [2] Analia N. Cillis and Diego D. Harari. Photon - graviton conversion in a primordial magnetic field and the cosmic microwave background. *Phys. Rev. D*, 54:4757–4759, 1996. [arXiv:astro-ph/9609200](#), [doi:10.1103/PhysRevD.54.4757](#).
 - [3] Chiara Caprini and Ruth Durrer. Gravitational waves from stochastic relativistic sources: Primordial turbulence and magnetic fields. *Phys. Rev. D*, 74:063521, 2006. [arXiv:astro-ph/0603476](#), [doi:10.1103/PhysRevD.74.063521](#).
 - [4] M. S. Pshirkov and D. Baskaran. Limits on High-Frequency Gravitational Wave Background from its interplay with Large Scale Magnetic Fields. *Phys. Rev. D*, 80:042002, 2009. [arXiv:0903.4160](#), [doi:10.1103/PhysRevD.80.042002](#).
 - [5] Salvatore Capozziello, Mohsen Khodadi, and Gaetano Lambiase. The quark chemical potential of QCD phase transition and the stochastic background of gravitational waves. *Phys. Lett. B*, 789:626–633, 2019. [arXiv:1808.06188](#), [doi:10.1016/j.physletb.2019.01.004](#).
 - [6] Mohsen Khodadi, Kouros Nozari, Habib Abedi, and Salvatore Capozziello. Planck scale effects on the stochastic gravitational wave background generated from cosmological hadronization transition: A qualitative study. *Phys. Lett. B*, 783:326–333, 2018. [arXiv:1805.11310](#), [doi:10.1016/j.physletb.2018.07.010](#).

- [7] Valerie Domcke and Camilo Garcia-Cely. Potential of radio telescopes as high-frequency gravitational wave detectors. *Phys. Rev. Lett.*, 126(2):021104, 2021. [arXiv:2006.01161](#), [doi:10.1103/PhysRevLett.126.021104](#).
- [8] Tomohiro Fujita, Kohei Kamada, and Yuichiro Nakai. Gravitational Waves from Primordial Magnetic Fields via Photon-Graviton Conversion. *Phys. Rev. D*, 102(10):103501, 2020. [arXiv:2002.07548](#), [doi:10.1103/PhysRevD.102.103501](#).
- [9] Pisin Chen and Teruaki Suyama. Constraining Primordial Magnetic Fields by CMB Photon-Graviton Conversion. *Phys. Rev. D*, 88(12):123521, 2013. [arXiv:1309.0537](#), [doi:10.1103/PhysRevD.88.123521](#).
- [10] Pisin Chen. Resonant photon-graviton conversion and cosmic microwave background fluctuations. *Physical review letters*, 74(5):634, 1995.
- [11] Alexander D. Dolgov and Damian Ejlli. Conversion of relic gravitational waves into photons in cosmological magnetic fields. *JCAP*, 12:003, 2012. [arXiv:1211.0500](#), [doi:10.1088/1475-7516/2012/12/003](#).
- [12] Alexander D. Dolgov and Damian Ejlli. Resonant high energy graviton to photon conversion at the post-recombination epoch. *Phys. Rev. D*, 87(10):104007, 2013. [arXiv:1303.1556](#), [doi:10.1103/PhysRevD.87.104007](#).
- [13] Emi Masaki and Jiro Soda. Conversion of Gravitons into Dark Photons in Cosmological Dark Magnetic Fields. *Phys. Rev. D*, 98(2):023540, 2018. [arXiv:1804.00458](#), [doi:10.1103/PhysRevD.98.023540](#).
- [14] Salvatore Capozziello, Amodio Carleo, and Gaetano Lambiase. The amplification of cosmological magnetic fields in extended $f(T,B)$ teleparallel gravity. *JCAP*, 10:020, 2022. [arXiv:2208.11186](#), [doi:10.1088/1475-7516/2022/10/020](#).
- [15] José A. R. Cembranos, Miguel González Ortiz, and Prado Martín-Moruno. Graviton-photon oscillation in a cosmic background for a general theory of gravity. 2 2023. [arXiv:2302.08186](#).
- [16] DJ Fixsen, A Kogut, S Levin, M Limon, P Lubin, P Mirel, M Seiffert, E Wollack, T Villela, et al. Arcade 2 measurement of the absolute sky brightness at 3–90 ghz. *The Astrophysical Journal*, 734(1):5, 2011.
- [17] Judd D. Bowman, Alan E. E. Rogers, Raul A. Monsalve, Thomas J. Mozdzen, and Nivedita Mahesh. An absorption profile centred at 78 megahertz in the sky-averaged spectrum. *Nature*, 555(7694):67–70, 2018. [arXiv:1810.05912](#), [doi:10.1038/nature25792](#).

- [18] Philipp P Kronberg. Extragalactic magnetic fields. *Reports on Progress in Physics*, 57(4):325, 1994.
- [19] P. A. R. Ade et al. Planck 2015 results. XIX. Constraints on primordial magnetic fields. *Astron. Astrophys.*, 594:A19, 2016. [arXiv:1502.01594](#), [doi:10.1051/0004-6361/201525821](#).
- [20] Karsten Jedamzik, Visnja Katalinic, and Angela V. Olinto. Damping of cosmic magnetic fields. *Phys. Rev. D*, 57:3264–3284, 1998. [arXiv:astro-ph/9606080](#), [doi:10.1103/PhysRevD.57.3264](#).
- [21] Tina Kahniashvili, Alexander G. Tevzadze, Axel Brandenburg, and Andrii Neronov. Evolution of Primordial Magnetic Fields from Phase Transitions. *Phys. Rev. D*, 87(8):083007, 2013. [arXiv:1212.0596](#), [doi:10.1103/PhysRevD.87.083007](#).
- [22] AM Taylor, Ie Vovk, and A Neronov. Extragalactic magnetic fields constraints from simultaneous gev–tev observations of blazars. *Astronomy & Astrophysics*, 529:A144, 2011.
- [23] Ruth Durrer and Andrii Neronov. Cosmological Magnetic Fields: Their Generation, Evolution and Observation. *Astron. Astrophys. Rev.*, 21:62, 2013. [arXiv:1303.7121](#), [doi:10.1007/s00159-013-0062-7](#).
- [24] Kandaswamy Subramanian. The origin, evolution and signatures of primordial magnetic fields. *Rept. Prog. Phys.*, 79(7):076901, 2016. [arXiv:1504.02311](#), [doi:10.1088/0034-4885/79/7/076901](#).
- [25] Damian Ejlli. Graviton-photon mixing. Exact solution in a constant magnetic field. *JHEP*, 06:029, 2020. [arXiv:2004.02714](#), [doi:10.1007/JHEP06\(2020\)029](#).
- [26] Cedric Deffayet, Diego Harari, Jean-Philippe Uzan, and Matias Zaldarriaga. Dimming of supernovae by photon pseudoscalar conversion and the intergalactic plasma. *Phys. Rev. D*, 66:043517, 2002. [arXiv:hep-ph/0112118](#), [doi:10.1103/PhysRevD.66.043517](#).
- [27] Yuval Grossman, Sourov Roy, and Jure Zupan. Effects of initial axion production and photon axion oscillation on type Ia supernova dimming. *Phys. Lett. B*, 543:23–28, 2002. [arXiv:hep-ph/0204216](#), [doi:10.1016/S0370-2693\(02\)02448-6](#).
- [28] Alessandro Mirizzi, Georg G. Raffelt, and Pasquale D. Serpico. Photon-axion conversion as a mechanism for supernova dimming: Limits from CMB spectral distortion. *Phys. Rev. D*, 72:023501, 2005. [arXiv:astro-ph/0506078](#), [doi:10.1103/PhysRevD.72.023501](#).
- [29] Nicola Bassan, Alessandro Mirizzi, and Marco Roncadelli. Axion-like particle effects on the polarization of cosmic high-energy gamma sources. *JCAP*, 05:010, 2010. [arXiv:1001.5267](#),

- doi:10.1088/1475-7516/2010/05/010.
- [30] Manuel Meyer, Daniele Montanino, and Jan Conrad. On detecting oscillations of gamma rays into axion-like particles in turbulent and coherent magnetic fields. *JCAP*, 09:003, 2014. arXiv:1406.5972, doi:10.1088/1475-7516/2014/09/003.
- [31] Carmelo Evoli, Matteo Leo, Alessandro Mirizzi, and Daniele Montanino. Reionization during the dark ages from a cosmic axion background. *JCAP*, 05:006, 2016. arXiv:1602.08433, doi:10.1088/1475-7516/2016/05/006.
- [32] Emi Masaki, Arata Aoki, and Jiro Soda. Photon-Axion Conversion, Magnetic Field Configuration, and Polarization of Photons. *Phys. Rev. D*, 96(4):043519, 2017. arXiv:1702.08843, doi:10.1103/PhysRevD.96.043519.
- [33] Giorgio Galanti and Marco Roncadelli. Behavior of axionlike particles in smoothed out domainlike magnetic fields. *Phys. Rev. D*, 98(4):043018, 2018. arXiv:1804.09443, doi:10.1103/PhysRevD.98.043018.
- [34] Francesco Schiavone, Daniele Montanino, Alessandro Mirizzi, and Francesco Capozzi. Axion-like particles from primordial black holes shining through the Universe. *JCAP*, 08:063, 2021. arXiv:2107.03420, doi:10.1088/1475-7516/2021/08/063.
- [35] M. Kachelriess and J. Tjemsland. On the origin and the detection of characteristic axion wiggles in photon spectra. *JCAP*, 01(01):025, 2022. arXiv:2111.08303, doi:10.1088/1475-7516/2022/01/025.
- [36] Georg Raffelt and Leo Stodolsky. Mixing of the photon with low-mass particles. *Physical Review D*, 37(5):1237, 1988.
- [37] Alessandro Mirizzi, Georg G. Raffelt, and Pasquale D. Serpico. Signatures of Axion-Like Particles in the Spectra of TeV Gamma-Ray Sources. *Phys. Rev. D*, 76:023001, 2007. arXiv:0704.3044, doi:10.1103/PhysRevD.76.023001.
- [38] Pierluca Carenza, Carmelo Evoli, Maurizio Giannotti, Alessandro Mirizzi, and Daniele Montanino. Turbulent axion-photon conversions in the milky-way, 2021. arXiv:2104.13935.
- [39] M. C. David Marsh, James H. Matthews, Christopher Reynolds, and Pierluca Carenza. Fourier formalism for relativistic axion-photon conversion with astrophysical applications. *Phys. Rev. D*, 105(1):016013, 2022. arXiv:2107.08040, doi:10.1103/PhysRevD.105.016013.
- [40] Eric D Carlson and W Daniel Garretson. Photon to pseudoscalar conversion in the interstellar medium. *Physics Letters B*, 336(3-4):431–438, 1994.

- [41] D. Ejlli and V. R. Thandlam, “Graviton-photon mixing,” *Phys. Rev. D* **99** (2019) no.4, 044022 doi:10.1103/PhysRevD.99.044022 [arXiv:1807.00171 [gr-qc]].
- [42] D. Ejlli, “Axion mediated photon to dark photon mixing,” *Eur. Phys. J. C* **78** (2018) no.1, 63 doi:10.1140/epjc/s10052-017-5506-1 [arXiv:1609.06623 [hep-ph]].
- [43] Tetsutaro Higaki, Kazunori Nakayama, and Fuminobu Takahashi. Cosmological constraints on axionic dark radiation from axion-photon conversion in the early Universe. *JCAP*, 09:030, 2013. arXiv:1306.6518, doi:10.1088/1475-7516/2013/09/030.
- [44] Kerstin E. Kunze and Miguel Á. Vázquez-Mozo. Constraints on hidden photons from current and future observations of CMB spectral distortions. *JCAP*, 12:028, 2015. arXiv:1507.02614, doi:10.1088/1475-7516/2015/12/028.
- [45] Ruth Durrer and Chiara Caprini. Primordial magnetic fields and causality. *JCAP*, 11:010, 2003. arXiv:astro-ph/0305059, doi:10.1088/1475-7516/2003/11/010.
- [46] Vittoria Demozzi, Viatcheslav Mukhanov, and Hector Rubinstein. Magnetic fields from inflation? *JCAP*, 08:025, 2009. arXiv:0907.1030, doi:10.1088/1475-7516/2009/08/025.
- [47] Tina Kahniashvili, Axel Brandenburg, Ruth Durrer, Alexander G. Tevzadze, and Winston Yin. Scale-invariant helical magnetic field evolution and the duration of inflation. *JCAP*, 12:002, 2017. arXiv:1610.03139, doi:10.1088/1475-7516/2017/12/002.
- [48] Axel Brandenburg, Ruth Durrer, Tina Kahniashvili, Sayan Mandal, and Weichen Winston Yin. Statistical Properties of Scale-Invariant Helical Magnetic Fields and Applications to Cosmology. *JCAP*, 08:034, 2018. arXiv:1804.01177, doi:10.1088/1475-7516/2018/08/034.
- [49] Tina Kahniashvili, Alexander G. Tevzadze, and Bharat Ratra. Phase Transition Generated Cosmological Magnetic Field at Large Scales. *Astrophys. J.*, 726:78, 2011. arXiv:0907.0197, doi:10.1088/0004-637X/726/2/78.
- [50] Tina Kahniashvili, Alexander G. Tevzadze, Shiv K. Sethi, Kanhaiya Pandey, and Bharat Ratra. Primordial magnetic field limits from cosmological data. *Physical Review D*, 82(8), oct 2010. URL: <https://doi.org/10.1103/PhysRevD.82.083005>, doi:10.1103/physrevd.82.083005.